FLIGHT LOADS RESEARCH OF TWIN VERTICAL TAIL FOR BLENDED WING-BODY AIRCRAFT BASED ON STRAIN GAUGE CAILBRATION

Zhengwang Guo, Ani Tang, Qideng Jing

Chinese Flight Test Establishment Aircraft Institute，Xi′an Shanxi,710089

Abstract

By completing 200 symmetrical maneuvers at different air pressure altitudes (15km~2km), different Mach numbers (including subsonic, transonic and supersonic speeds), and different normal load coefficients (from minimum negative overload to maximum positive overload) at the center of mass of the aircraft, as well as opening the speed brake during low-altitude subsonic horizontal straight line flight, the bending moment, torsional moment and shear force of the left and right parts of the double vertical tail of the testing aircraft with advanced aerodynamic layout were measured by strain method, and the load on double vertical tail was analyzed. The results show that symmetrical maneuvering is an important load condition unique to double vertical tails, and the load on one side of the vertical tail can reach 60% of the design limit load. When the speed brake is opened, the load increases by 1.5~3 times, and when a single factor changes, the bending moment and shear force increase with the increase of the total lift coefficient, and there is an obvious regularity with the Mach number.

Keywords: twin vertical tail; loads; symmetrical maneuver; the total lift coefficient; Mach number.

Introduction

While ensuring the stability of the aircraft's lateral side, it can improve the control efficiency and easily meet the needs of survivability, so that the twin vertical tail has become the mainstream layout form of the third and fourth generation fighters [1]. When the aircraft is flying in symmetrical maneuver, the load on vertical tail is almost 0 due to the symmetry of the flow field on both sides of the single vertical tail arranged on the symmetrical plane of the aircraft [2-5]. For the twin vertical tail with symmetrical arrangement relative to the aircraft, due to the asymmetry of the inner flow field and the outer flow field of the left and right parts of the unilateral vertical tail, there is a load on each side of the vertical tail during symmetrical maneuvering[6,7], and it changes with the different influences of the aircraft precursor on the vertical tail flow field, as well as the different combinations of various factors such as flight speed pressure and Mach number. Russia attaches great importance to this new load situation of the twin vertical tail when studying the flight load [8,9].

In order to study this load characteristics of twin vertical tail, strain method was used to measure the twin vertical tail loads of a certain blended wing-body aircraft with advanced aerodynamic layout including bending moment, torsional moment and shear force of different sections. Completed approximately 200 symmetrical maneuvering flights in different states represented by the air pressure altitude, Mach number and normal load coefficient at the center of mass , as well as the shape change of the aircraft precursor during low-altitude straight flight (by opening the fuselage speed brake). Obtained the loads of the twin vertical tails in these flight states. For the first time in China, analysised and studied the quantitative of the measured loads of twin vertical tail and revealed the regularity of the loads, which has an important reference for the design and verification of the twin vertical tail and its related structures of the blended wing-body aircraft, as well as the

development of the domestic twin vertical tail aircraft.

Since 1953, the method of structural loads measurement by strain gauge was first outlined in the literature as a NASA report [10] and, later, repeatedly applied in tests on aircraft structures [11-14], the method has been developed for more than half a century[15,16]. With the change of aircraft structure [15-20] and the development of sensor systems [21-25], strain method load measurement is also constantly developing. However, the method for aircraft structural loads measurement with electrical strain gauges is still the most reliable method up to now [26-28].

1 Test aircraft

The testing aircraft is normal pneumatic layout with blended wing-body, the wide flat fuselage and the medium-aspect ratio backswept wing with chine and lifters in leading and trailing edge are fused into a complete lift body. It has double fins and rudders, and low-mounted differential all movable horizontal tail. The upper part of the front fuselage has a single airbrake with a large deflection angle. Two turbojet engines are installed in two compartments in the rear fuselage, the longitudinal axis of which is parallel to the aircraft's axis of symmetry. See Figure 1.

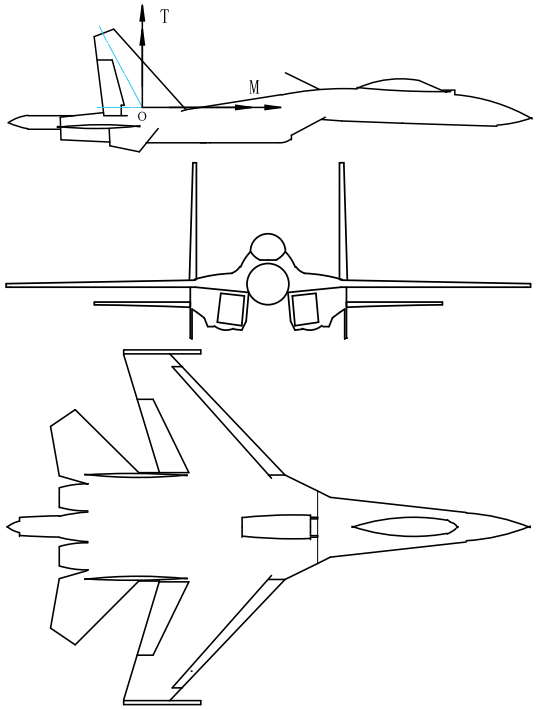

Figure 1- Layout of the testing aircraft.

The twin vertical tail has a large sweep angle on the leading edge, the relative wing area is 0.262, the aspect ratio and root-tip ratio are 1.63 and 3.78, respectively, and the inclination angle is 0º. The vertical tail is fixed to the side members of the fuselage frame by two joints at the lower end of the spar and consists of a frame, wall plates, wing tips, dorsal fin, and lower wall plates. The frame includes: front and rear beams, side ribs, wing ribs, front ribs, walls, leading edge partitions, front edge strips, and rear edge strips. The beam profile is I-shaped, consisting of the root (steel die forging) and the outer section (aluminum alloy die forging). The siding is a glue rivet structure, which is composed of an aluminum alloy skin and an aluminum alloy long truss with an I-shaped section.

2 Loads measurement by strain method

To measure the structural loads of an aircraft by strain gauge method, strain gauge bridges should be installed on the load measurement structure on the basis of structural force analysis, and the main load cases in the flight should be simulated, then the loads should be applied to the structure and calibrated. The loads model represented by the following formula should be established [15,26,27].

$$F = \sum_{i=1}^{n} \alpha_i \varepsilon_i$$

Where F is the structural loads, including bending moment, torsional moment, and shear force; ε is the strain gauge bridge readings; α is the load factor, which is determined when the loads calibration test is finished; n denotes the number of bridges. The key steps of load measurement by strain gauge include strain gauge installation, load calibration test, and load modeling.

2.1 Strain gauge Installation

According to the structural characteristics of the twin vertical tail and the analysis of structural force and deformation, considering the feasibility and ease of aircraft modification construction, the number of load measurement sections in the left and right vertical tails is set to be 5 and 3 respectively (see Fig. 2).

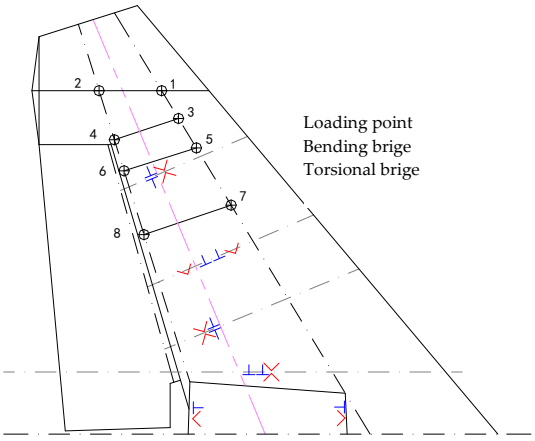

Figure 2-Load measurement sections and strain gauge installation position.

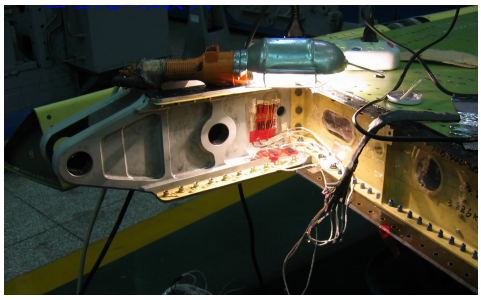

a) Strain gauges in the root of the vertical tail rear beam

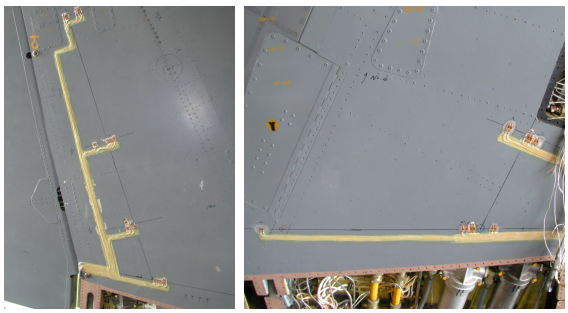

b) Strain gauges on outer section

Figure 3-Strain gauges on the vertical tail.

The strain gauge bridges, which measure the bending moment, torsional moment, and shear force of the root section, are installed on the flange and web of the beam, and the strain gauge bridges, which measure the bending moment, torsional moment, and shear force of each section of the wing surface, are installed along the rigid shaft on the inner wing surface (see Fig. 3).

2.2 Load calibration test

Load calibration refers to simulating the actual loads of the aircraft, applying known loads to the structure with strain gauge bridges, and obtaining the original data of load modeling. The important contents of load calibration test include determining the load cases, constraint and fixation of aircraft, and loading implementation.

According to the characteristics of the twin vertical tail structure, load is applied to the left and right vertical tails at the same time by self-balancing loading mode[29] (see Fig. 4). The load situation include 8 kinds of self-balancing point loads, that means, the two points corresponding to the left and right vertical tail positions (X and Y coordinates are the same) was simultaneously applied the same amount of calibration load to the outside, and the specific position is shown in Figure 1. The maximum load at each loading point is shown in Table 1. Considering that the self-balancing loading is adopted, the overall balance state of the aircraft is not changed, and the aircraft does not need to be specially fixed when applying the load, but the aircraft is pushed off the ground with three fuselage jacks, so that the landing gear wheels are not affected by the ground support reaction.

Table 1 - Maximum calibration load at each loading point

Loading point	1	2	3	5	6	7	8
load	0.45	0.45	0.64	1.08	0.99	1.8	1.86

Figure 4-Twin vertical tail loading calibration test.

2.3 Load Modeling

2.3.1 Basic Methods of Modeling

The theoretical basis of load calibration test is the linear superposition principle between force and strain, that means, in elastic range, strain and load are linearly related, and the structural strain is the sum of the strains caused by all loads. For the vertical tail, when the structure is bent and torsionally deformed, the reading of the strain gauge bridge modified on the vertical tail is the result of the comprehensive effect of shear force, bending moment and torsional moment. Considering that the bending moment, torsional moment is generated by shear force, ie：

$$M = VY, \quad T = VX \tag{1}$$

Then any bridge's reading can be expressed as a power polynomial:

$$\varepsilon_i = \alpha_{i1}V + \alpha_{i2}VX + \alpha_{i3}VY + \alpha_{i4}VXY + \alpha_{i5}VX^2 + \alpha_{i6}VY^2 + \ldots + \alpha_{ij}VXY^s \tag{2}$$

J different bridge's readings are expressed as matrices as:

$$\begin{Bmatrix}\varepsilon_1\\ \varepsilon_2\\ \varepsilon_3\\ .\\ .\\ .\\ \varepsilon_j\end{Bmatrix}=\begin{bmatrix}\alpha_{11} & \alpha_{12} & \alpha_{13} & ..... & \alpha_{1j}\\ \alpha_{21} & \alpha_{22} & \alpha_{23} & ..... & \alpha_{2j}\\ \alpha_{31} & \alpha_{32} & \alpha_{33} & ..... & \alpha_{3j}\\ . & . & . & ..... & .\\ . & . & . & ..... & .\\ . & . & . & ..... & .\\ \alpha_{j1} & \alpha_{j2} & \alpha_{j3} & ..... & \alpha_{jj}\end{bmatrix}\begin{Bmatrix}V\\ VX\\ VY\\ .\\ .\\ .\\ VX^rY^s\end{Bmatrix} \quad (3)$$

In the above equation, if the determinant of the coefficient matrix is not 0, then equation 3) left multiplied by the inverse matrix of the coefficient matrix, and taking the first three rows, formula 4) can be obtained.

$$\begin{Bmatrix}V\\ VY\\ VX\end{Bmatrix}=\begin{Bmatrix}V\\ M\\ T\end{Bmatrix}=\begin{bmatrix}\beta_{11} & \beta_{12} & \beta_{13} & ..... & \beta_{1j}\\ \beta_{21} & \beta_{22} & \beta_{23} & ..... & \beta_{2j}\\ \beta_{31} & \beta_{32} & \beta_{33} & ..... & \beta_{3j}\end{bmatrix}\begin{Bmatrix}\mu_1\\ \mu_2\\ \mu_3\\ .\\ .\\ .\\ \mu_j\end{Bmatrix} \quad (4)$$

The physical meaning of equation (4) is that the load can be expressed as a linear function of the reading of the strain gauge bridges, which is the linear load model commonly used in load measurement. Based on the data of loads and strain bridge readings obtained by load calibration test, the coefficient βij of different loads of different section can be determined according to the principle of least squares, that is, the load model can be established, and the accuracy of the model can be tested.

Theoretically, only 3 strain bridges and 3 load cases are required to solve equation 4), but due to the complexity of the structure and the coupling of various loads, the load model obtained with 3 bridges and 3 load cases usually has a large error. Before load modeling, the bridge characteristics should be analyzed to select the optimal bridges for load modeling. Bridge characterization analysis includes repeatability, stability, sensitivity, linearity, and load characteristics analysis. The load characteristics are analyzed by the response coefficient, which refers to the strain caused by the unit load[15,26], and the change of the response coefficient along the chordwise and spanwise characterizes the load characteristics of the bridge.

Fig. 5 shows the variation curve of the response of the root section strain gauge bridges with load when loaded on point 3. It can be seen from the graph that the response of each strain gauge bridge has good repeatability and stability, and has good linearity with the load. Fig. 6 show the response coefficient curves of two bridges at the root of the left vertical tail on rear beam respectively, and a) is bending bridge LCW20, b) is shear bridge LCW21. It can be seen from figure a) that when loaded on the front beam (1, 3, 5, 7 points) and rear beam (2, 6, 8 points) respectively, the response of bridge LCW20 increases linearly with the increase of the radial coordinates, showing its bending moment characteristics. At the same time, the response of the bridge varies with the tangential coordinates, indicating that it is also affected by torsional moment and sensitive to the load of the front beam. As can be seen from figure b), LCW21 is also affected by bending moment and torsional moment, and is sensitive to the load of the rear beam.

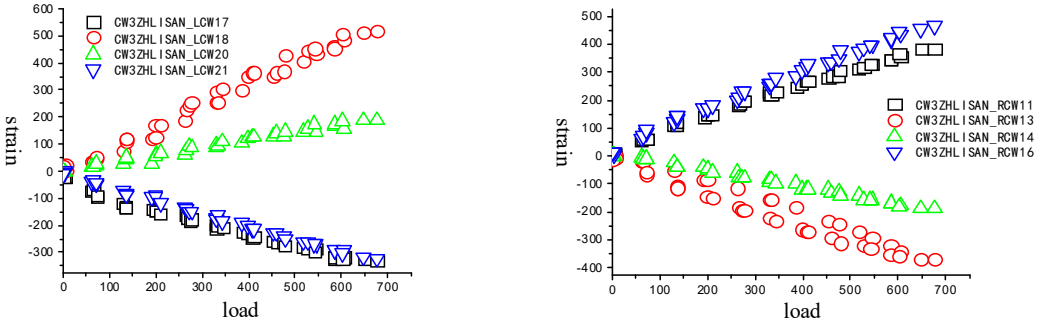

Figure 5 - Variation curves of the response of strain bridges on root with load

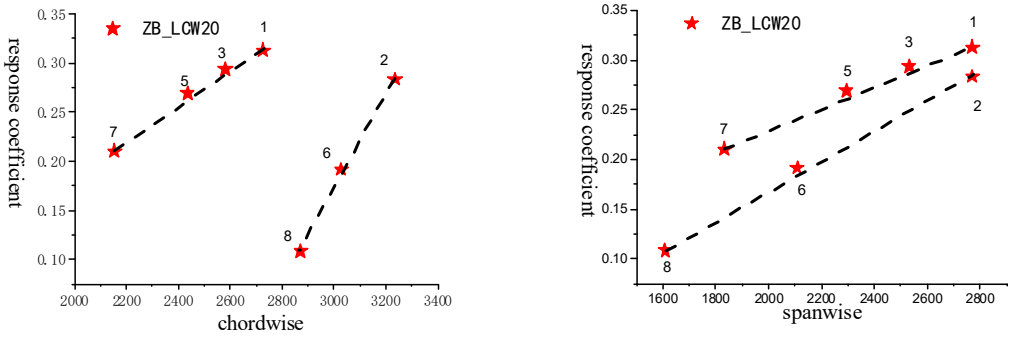

a) response coefficient curve of bending moment bridge LCW20

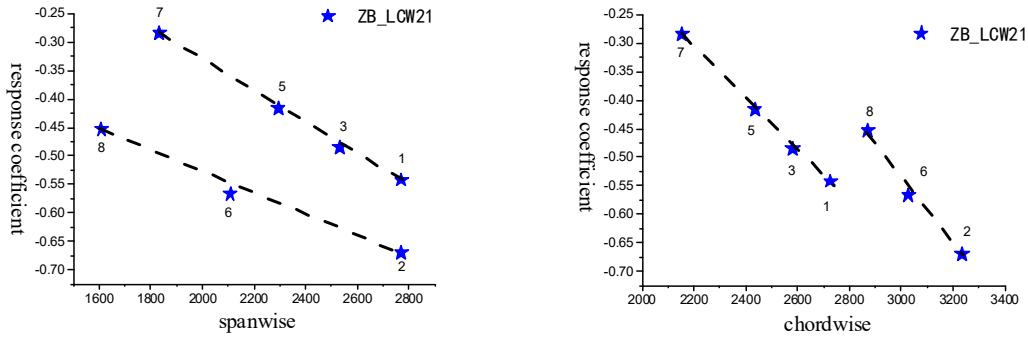

b) Response coefficient curve of shear bridge LCW21

Figure 6 - Response coefficient curve of some strain bridges on vertical tail

2.3.3 Load model

Through the above analysis, it can provide a basis for the selection of strain gauge bridges with different properties for load modeling, and the load model for flight measurement can be obtained by using multiple linear regression. Table 2 shows the loads model for the vertical tail root section.

Table 2 - Load model of root section

	brige / load	LCW20	LCW21	LCW17	LCW18	Calibration error(%)
Left tail	M	3595.45	-1605.3	-936.23	0	-1.88
	T	-174.51	-2722.3	1407.51	0	-3.61
	V	5.5236	-3.1882	0	1.3892	-1.58
	brige / load	RCW13	RCW14	RCW11	RCW16	Calibration error (%)
Right tail	M	-87.22	-5133.1	0	1039.87	-3.09
	T	1.35	524.67	-1608.5	2379.99	0.11
	V	-4.4309	0	-4.1122	1.3676	1.26

3 Flight Test and analysis

3.1 Flight Test Status

Flight tests include symmetrical maneuvers and asymmetric maneuvers, and this article only describes symmetrical maneuvers. Symmetrical maneuvers are performed at air pressure altitudes of 15、10、5、2kilometers.The Mach number is limited to the flight envelope of the aircraft at each altitude, ranging from subsonic, transonic to supersonic speeds. The normal load coefficient at the center of mass of the aircraft is limited to the strength envelope of the aircraft, from the minimum negative overload to the maximum positive overload. A total of 200 maneuvering flights were completed. The specific status points are shown in Figure 7, (the vertical axis in the figure is the measured value of load factor divided by the maximum load factor). In order to study the effect of the airframe airbrake, the airbrake was opened when flying in a straight line at subsonic speed at low altitude

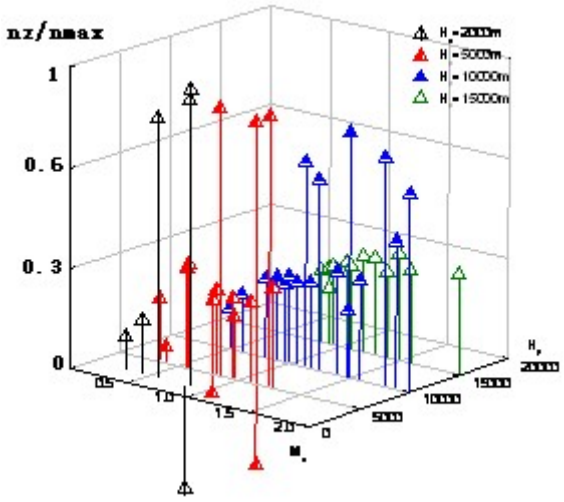

Figure 7 - Flight test status of symmetrical maneuvering.

3.2 Data Processing

3.2.1 Load and parameter calculation

The measured structure strain of the left and right parts of the twin vertical tail during flight test were substituted into the load equations (1) established by load calibration test, the flight loads of both tail can be obtained. In loads analysis, the load direction of the left and right parts of the twin vertical tail is the same, that is, the shear force is positive when the lateral force is directed to the right, and the bending moment and torque are positive in the direction of their vector and the direction of the reference axis (see Fig. 1). The load value is expressed in the dimensionless form

of the ratio of the measured value to the design limit value, and the ratio of the measured value to the measured maximum value of lateral maneuvering. The measured bending moment, torque, and shear force are respectively expressed in dimensionless form divided by q·1m3、q·1m3、q·1m2.In addition, the following calculations were made:

① Let the normal force be equal to the lift force [5], and the total lift coefficient of the aircraft is calculated according to Eq. (5).

$$C_{La} = n_z(W_0 + \Delta W)/qS_w \tag{5}$$

where nz、W0、ΔW、q、and Sw are the normal load coefficient of the aircraft's centroid, the empty weight, the additional weight caused by fuel and external loading, the flight speed pressure, and the wing area respectively.

② Use Equation (6) to dimensionless processing of the roll angle rate, pitch angle rate and yaw angle rate of the aircraft [6]:

$$\bar{\omega}_x = \frac{\omega_x \cdot l_a}{2V_t}, \bar{\omega}_y = \frac{\omega_y \cdot b_a}{V_t}, \bar{\omega}_z = \frac{\omega_z \cdot l_a}{2V_t} \tag{6}$$

where l_a、b_a、V_t are the wingspan length, the average aerodynamic chord length, and the true speed of the aircraft.

③ Calculating the three-direction angular acceleration rate of the aircraft by equation (7) obtained by digital differentiation [7]

$$\dot{\omega}(t_i) = \frac{1}{\Delta t}\sum_{j=1}^{m} k_j[\omega(t_{i+j}) - \omega(t_{i-j})] \tag{7}$$

Where m is the number of data taken to calculate the angular acceleration rate forward (backward) at the time of calculation, kj is a constant and is determined by equation (8).

$$k_j = \frac{25(3m^4 + 6m^3 - 3m + 1)j - 35(3m^2 + 3m - 1)j^3}{m(m+1)(m+2)(m-1)(2m-1)(2m+1)(2m+3)} \tag{8}$$

④ Using the linear regression model (9), to identify and analysis the main influencing factors of the loads

$$F = F_0 + k_{C_{L\alpha}} C_{L\alpha} + k_\beta \beta + k_\delta \delta + k_{\bar{\omega}_x} \bar{\omega}_x + k_{\bar{\omega}_z} \bar{\omega}_z + k_{\dot{\bar{\omega}}_x} \dot{\bar{\omega}}_x + k_{\dot{\bar{\omega}}_z} \dot{\bar{\omega}}_z \tag{9}$$

Where F and F0 are the load and constant terms; $k_{C_{L\alpha}}$、k_β、k_δ、$k_{\bar{\omega}_x}$、$k_{\bar{\omega}_z}$ are the regression coefficients; $k_{\dot{\bar{\omega}}_x}$、$k_{\dot{\bar{\omega}}_z}$ are the sideslip angle and rudder declination angle

3.2.2 Data selection of symmetrical maneuver

The ideal symmetrical maneuvering flight is the movement around the horizontal axis of the aircraft, excluding the transverse lateral movement. Since it is unrealistic to choose a purely symmetrical maneuver in flight measured data. For this reason, different tolerances are set for different flight parameters. Ignores the transverse and lateral motion of the aircraft within the tolerance. The main control conditions are as follows

① Roll angle：$|\varphi| \le 3°$；

② Roll angle rate：$|\omega_x| \le 1°/s$；

③ sideslip angle：$|\beta| \le 0.3°$；

④ Yaw angle rate：$|\omega_z| \le 0.2°/s$；

⑤ Lateral load coefficient at the center of mass：$|n_y| \le 0.1$；

⑥ Yaw maneuver displacement：$|D_r| \le 15mm$。

3.3 Measured load extremes

Fig. 8 shows the extreme values of the measured loads of the vertical tail on one side at four different altitudes, and table 3 shows the maximum load value and the corresponding flight state (where the Mach number is the measured value divided by the maximum Mach number, and the load factor is the measured value divided by the maximum load factor).

It can be seen from Fig. 8 and Table 3 that the maximum value of unilateral vertical tail bending moment and shear force occurs at low altitude and transonic speed. The maximum torque occurs at middle altitude the and transonic maneuvers, and the magnitude reaches 64%, 60% and 64% of the design limits loads, respectively, and 77%, 77% and 94% of the measured maximum values of the lateral maneuvering loads. So in symmetrical maneuvering, the unilateral load of the twin vertical tail is very serious.

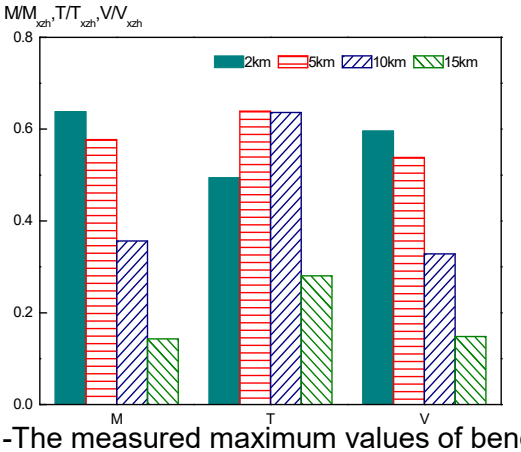

Figure 8 -The measured maximum values of bending moment M, torque N, and shear force V at different heights.

Table 3 - Maximum state of vertical tail loads on one side of symmetrical maneuver

	H_p	M_a /M_{amax}	n_z / n_{zmax}	α	measured /limit	measured / measured max
M	2069	0.45	0.93	5.3	0.64	0.77
T	4944	0.62	0.65	3.1	0.64	0.94
V	2078	0.43	0.98	4.8	0.60	0.77

3.4 Factors influencing Load

3.4.1 Opening the airbrake

Fig. 9 shows the measured bending moment, torque and shear force history of the left and right parts of the twin vertical tail when the airbrake on the airframe is turned on in a straight flight at subsonic speed and the air pressure altitude hp is about 3000 meters (SSBO is the airbrake state). It can be seen from the figure that when the airbrake is opened to the maximum angle, the bending moment, shear force and torque on one side of the vertical tail can be increased to 3 times, 2.5 times and 5 times of the load when the airbrake is closed, respectively, reaching 42%, 38% and 9% of the design limit loads, and 50%, 49% and 13% of the measured maximum value of lateral maneuvering load. The increment of bending moment and shear force point to the symmetry plane of the aircraft. It can be seen that the influence of opening the airbrake on the unilateral load of the twin vertical tail is serious.

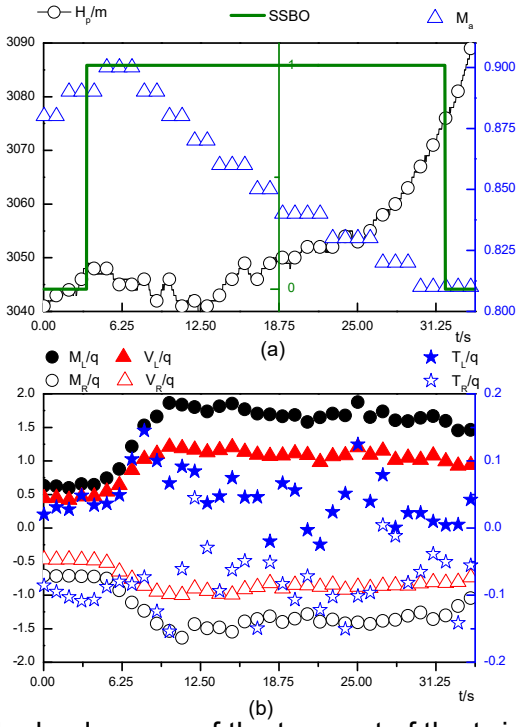

Figure 9-The load course of the two-part of the twin vertical tail during the speed brake opening.

3.4.2 Lift coefficient

Fig. 10a), b）, and c) respectively show that when the Mach number is relatively fixed, the variation of the measured bending moment, torque, and shear force of the left vertical tail with the lift coefficient in the three ranges of subsonic, transonic and supersonic speeds, respectively. It is known from the picture

1) When the Mach number Ma is constant, the bending moment increases with the increase of the lift coefficient CLa, and the linear correlation with the lift coefficient changes from strong to weak from supersonic speed, transonic speed to subsonic speed (the correlation coefficients of Ma and CLa are: 0.9969, 0.9860, 0.9848, respectively)

2) When the Mach number Ma is constant, the shear force V increases with the increase of the lift coefficient CLa, and the linear correlation of the shear force V with the lift coefficient CLa changes from strong to weak from supersonic to transonic to subsonic (the correlation coefficients between shear force and lift coefficient are: 0.9963, 0.9825, 0.9250, respectively). This law is the same as that of bending moments.

3) When the Mach number Ma is constant, the torque T only increases with the increase of the lift coefficient at supersonic speed, and is linearly correlated. There is no linear correlation in transonic and subsonic velocity (correlation coefficients between torque and lift coefficient are: 0.9888, -0.2044, 0.6959, respectively)

4) When the lift coefficient CLa is the same, the bending moment and shear force are the maximum in transonic speed, followed by subsonic speed, and the smallest for supersonic speed; Torque is different, with supersonic velocity being the maximum, transonic velocity being secondary, and subsonic velocity being the smallest.

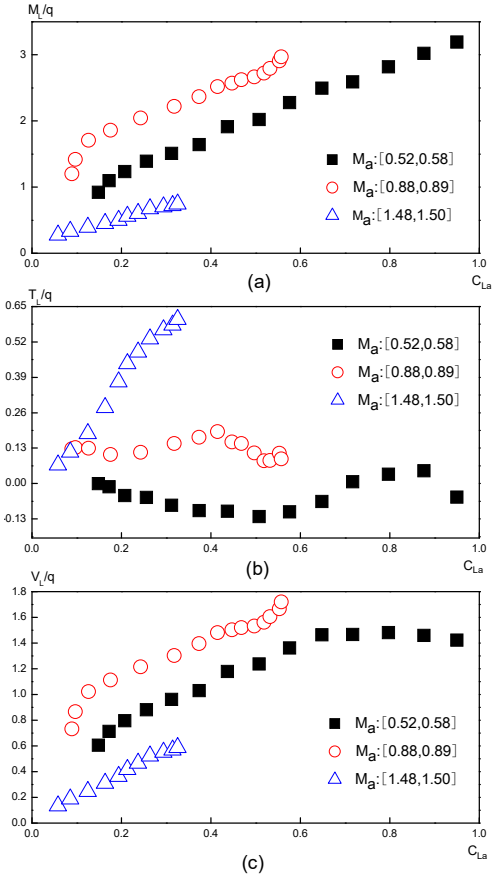

Figure 10 - Load variations with lift coefficient.

3.4.3 the Mach number

Fig. 11a), b), and c) respectively show the changes of measured bending moment, shear force, and torque in the left and right parts of the double vertical tail under the four conditions when the lift coefficient CLa is relatively fixed. As can be seen:

① When the lift coefficient is constant, the bending moment and shear force have obvious regularity with the Mach number Ma, and can be fitted by the third polynomial. At subsonic the bending moment and shear force increases with the increase of Mach number, reaches maximum at transonic (or high subsonic) speeds, and decreases at supersonic speeds.

② When the lift coefficient is constant, there is no obvious regularity between torque and Mach number; The magnitude (algebraic) seems to increase with the increase of the Mach number, and the trend weakens when the velocity reaches transonic speed

③ When the Mach number is the same, the bending moment and shear force increase with the increase of the lift coefficient, and the relationship between torque and lift coefficient is not obvious

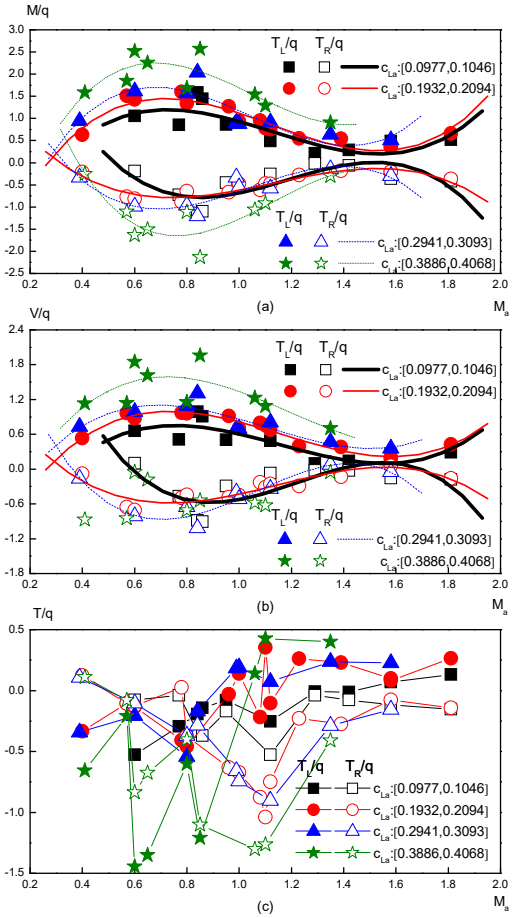

Figure 11 - Load variations with Mach number

3.5 Discuss

In sections 3.4.2 and 3.4.3, the analysis mainly focuses on the magnitude and influencing factors. As for the direction of the loads of the two parts of the twin vertical tail, it is obvious from the figure specified in section 3.2.1, that is, the load direction of the vertical tail on both sides is opposite when the symmetrical maneuver is carried out, points to (or deviates from) the symmetrical plane of the aircraft at the same time. As a whole, the resultant force of the two parts is very small. The resultant load of the twin vertical tail is not zero, which may be caused by the inherent asymmetry of the aircraft and the data tolerance taken. A large number of flight results show that this asymmetry becomes more pronounced with the increasing growth of the lift coefficient $C_{L\alpha}$.

4 Conclusion

The strain method was used to measure the flight load of the twin vertical tail, and the results were reliable. Studies have shown that symmetrical maneuvers of hybrid wing-body aircraft:

(1) The bending moment, shear force and torque on one side of the twin vertical tails can reach 64%, 60% and 64% of the design limit loads, which appear in the mid- and low-altitude transonic region;

(2) When the fuselage airbrake is turned on to change the shape of the front body of the fuselage, the unilateral load of the twin vertical tail increases by 1.5~3 times, and the bending moment, shear force and torque can reach 42%, 38% and 9% of the design limit loads.

(3) Flight speed pressure, total lift coefficient and Mach number are the main factors affecting the loads. When a single factor changes, the unilateral bending moment and shear force of the twin

vertical tail increase with the increase of the lift coefficient, and there is an obvious law with the Mach number. The law among torque, lift coefficient and Mach number is weak;

(4) Symmetrical maneuvering is an important load condition unique to twin vertical tails, which affects the strength and life of vertical tails and related structures. The quantitative analysis results in this paper can provide a reference for the design of wing-body fusion double-tail aircraft.

5 Contact Author Email Address

tangani@sohu.com

6 Copyright Statement

References

[1] Fang Baorui. *Aeroplane aerodynamic layout design* . 1st edition, Aviation Industry Press, 1997.

[2] *Practical aerodynamics of motor aircraft*. Command of the Chinese People's Liberation Army,1975.

[3] Barrett D. Flansburg. Structural loads analysis of a hybrid wing body transport. AIAA 2017-0205*58th AIAA/ASCE/AHS/ASC Structures,Structural Dynamics,and Materials Conference,* 9-13 January 2017,Grapevine, Texas,https://doi.org/10.2514/6.2017-0205.

[4] Ted L. Lomax. *Structural loads analysis for commercial transport aircraft.* American Institute of Aeronautics and Astronautics, 1996.

[5] Hou Zongtuan, Guo Zhaodian. Vertical tail flight loads design on large aircraft.*System Simulation Technology*， Vol.10, No.3,239-244,2014.7.

[6] P. VA. Acquiring tail load spectra from in-flight measurements.*34th Structures, Structural Dynamics and Materials Conference*, La Jolla,CA,U.S.A., 1993.

[7] Arturo J. Delgado-Gutiérrez, Michael J. Candon,Pier Marzocca and Oleg Levinski.Aerodynamic loads estimation on a twin vertical-tail configuration based on the single-step lattice boltzmann method simulation. *AIAA SCITECH 2024 Forum*, AIAA 2024-0062, Orlando, FL,https://doi.org/10.2514/6.2024-0062,2024.

[8] Клячко М. Д. ,Арнаутов Е. В. Летные прочностные испытания самолетов. *Статические нагрузки*: Спровочник:-М: Машиностроение, 1985.

[9] Ю.И.Снешко.*ИССЛЕДОВАНИЯ В ПОЛЕТЕ УСТОЙЧВОСТИ И УПРАВЛЯЕМОСТИ САМОЛЕТА.* МОСКВА:ИЗДАТЕЛЬСТВО “Машиностроение” ,1971.

[10] Skopinski, T.,Aiken, W.,Huston, W. Calibration of strain-gauge installation in aircraft structures for the measurements of flight loads.*NACA Technical Note 2993*. NACA: Washington, DC, USA, 1953.

[11] Jerald M. Jenkins, Albert E.Kuhl and Alan L. Carter. Strain gage calibration of a complex wing„*Journal of Aircraft*, Volume 14, No.12, pp. 1192–1196,1977.

[12] Eckstorm, C. Flight loads measurements obtained from calibrated strain-gage bridges mounted externally on skin of low-aspect-ratio wing. *NASA TN D-8349*, NASA: Washington, DC, USA, 1976.

[13] Hovell, P.,Webber, D., Roberts, T. The use of calibrated strain gauges for flight load determination. *Aeronautical Research Council Technical Report 1041*,NASA: Washington, DC, USA, 1969.

[14] Monaghan, R.,Fields, R. Experiments to study strain-gage load calibrations on wing structure at elevated temperatures. *NASA TN D-7390*. NASA: Washington, DC, USA, 1973.

[15] Jenkins, J.,DeAngelis, V. A summary of numerous strain-gauge load calibrations on aircraft wings and tails in a technology format. *NASA Technical Memorandum 4804*.NASA: Washington, DC, USA, 1997.

[16] Lokos, W.,Stauf, R. Strain-gage calibration parametric study. *NASA TM 212853*.NASA: Washington, DC, USA, 2004.

[17] Łukasz Swi ˛ech. Calibration of a load measurement system for an unmanned aircraft composite wing based on fibre Bragg gratings and electrical strain gauges. *Aerospace,* Vol.7, No. 3, 27,2020.

[18] Eric J. Miller,Francisco Pena,Ashante Jordan, Larry Hudson and William Lokos. Evaluation of wing load calibration and sensing methods using conventional strain gages and a fiber optic sensing system installed on a straight tapered wing,AIAA 2019-0227.*AIAA Scitech 2019 Forum*，*Session: Aircraft Structural Design, Test and Analysis*,San Diego, California, 2019.

[19] Halide Goknur Aydogan, Haytham Fayek, Xiuzhen Zhang, Michael Scott, Pier Marzocca, Kate Niessen, Daniel Franke and Oleg Levinski. Loads estimation from calibration test with machine learning,AIAA 2023-1707.*AIAA SCITECH 2023 Forum*,*Session: Topics in Structural Dynamics II*,National Harbor, MD, 2023.

[20] William A. Lokos, Eric J. Miller, Larry D. Hudson, Andrew C. Holguin, David C. Neufeld and Ronnie Haraguchi. Strain gage loads calibration testing with airbag support for the gulfstream III subsonic research aircraft testbed (SCRAT),AIAA 2015-2020.*53th Aerospace Science meeting,Session: Advances in Test Techniques, Test Management, & EFD/CFD Integration*,Kissimmee, Florida*,* 2015.

[21] Ramly, R.; Kuntjoro, W.; Rahman, M.K.A. Using embedded fiber bragg grating (FBG) sensors in smart aircraft structure materials. *Procedia Eng*, 41, 600–606,2012.

[22] Tserpes, K.I., Karachalios, V., Giannopoulos, I., Prentzias, V., Ruzek, R. Strain and damage monitoring in CFRP fuselage panels using fiber bragg grating sensors. *Part I: Design, manufacturing and impact testing, Compos. Struct*,107, 726–736, 2014.

[23] R ˚užek, R.,Kudrna, P. Kadlec, M., Karachalios, V., Tserpes, K. Strain and damage monitoring in CFRP fuselage panels using fiber bragg gr;ating sensors. *Part II: Mechanical testing and validation. Compos. Struct*. 107, 737–744, 2014.

[24] Ryu, C., Lee, J., Kim, C., Hong, C. Buckling behavior monitoring of composite wing box using multiplexed and multi-channeled built-in fiber bragg grating strain sensor. *NDT&E Int*, 41, 534–543, 2008.

[25] Ma, Z., Chen, X. Fiebr bragg gratings sensors for aircraft wing shape measurement: recent applications and technical analysis. *Sensors*,Vol. 19, No. 1, 55, 2019.

[26] Nicolas, M., Sullivan, R.W.,Richards, W.L. Large scale applications using FBG sensors: determination of in-flight loads and shape of a composite aircraft wing. *Aerospace*,Vol. 3, No.3, 18,2016.

[27] Guo ZhengWang. *Loads and Strength Flight Test of Aircraft*. 1st edition,Aviation Industry Press, 2018.

[28] Tedl. Lomax. *Civil transport aircraft structural load flight: Principles and Practices*, Aviation Industry Corporation of China, Project AE100 Management Office,1998.

[29] Guo Zhengwang. Self-balancing load calibration on aircraft twin-finned tail.*Structure & Environment Engineering,* Vol. 36, No. 4, 19-23,2009.